eurasia

Synergistic Effects of CuO Nanoparticles in MgO Powder for Enhanced Supercapacitor Performance

Article history:
Received : 13.06.2025
Revised : 26.11.2025
Accepted : 07.12.2025
Published : 30.06.2026

Poonam Negi[a], Naveen Chandra Joshi[b], Richa Saxena[c], Bhupendra Singh Rawat[d*]

Abstract: The incorporation of metal oxide nanoparticles into magnesium oxide (MgO) powder enhances its supercapacitor performance. This study investigates the influence of cooper oxide nanoparticles (CuO-NPs) incorporated into magnesium oxide (MgO) powder on the electrochemical performance of supercapacitors. Magnesium oxide (MgO), Copper Oxide nanoparticles (CuO-NPs), and their composite (MgO/CuO) were synthesized and evaluated under both three- and two-electrode configuration. Structural, morphological, and electrochemical characterizations were performed to assess the effect of CuO addition. X-ray diffraction (XRD) and scanning electron microscopy (SEM) confirmed the successful integration of CuO into the MgO matrix, accompanied by notable changes in crystallinity and particle morphology. Electrochemical performance was evaluated using cyclic voltammetry (CV), galvanostatic charge-discharge (GCD), and electrochemical impedance spectroscopy (EIS). The MgO/CuO composite demonstrated a markedly enhanced specific capacitance of 444.4 F/g at 2 A/g in a three-electrode system, significantly higher than individual MgO and CuO. The composite retained 96.8% capacitance after 5000 GCD cycles, showing excellent cyclic stability. EIS results revealed low series resistance, fast ion diffusion, and improved charge-transfer kinetics. The enhanced performance is attributed to the synergistic interaction between MgO and CuO, which improves surface activity, electron transport, and structural stability, thereby establishing MgO/CuO as a promising, cost-effective, and environmentally benign electrode material for next-generation high-performance supercapacitors.

Keywords: Supercapacitor, metal-oxide composite, specific capacitance, cyclic stability, electrochemical impedance spectroscopy

[a]Department of Chemistry, GRD Institute of Management & Technology, Dehradun, India

[b]Department of Chemistry, Graphic Era Deemed to be University, Dehradun, India

[c]Department of Physics, Shri Guru Ram Rai University, Dehradun, India

[d]Department of Physics, Uttaranchal Institute of Technology, Uttaranchal University, Dehradun, India

***Corresponding Author's Email**
dr.roselin@gmail.com

© The Author(s), 2026

1. INTRODUCTION

Energy storage technologies such as batteries and conventional capacitors are limited by low power density, restricted capacitance, slow-discharge rates, and environmental concerns (Naderi et al., 2020; Sohouli et al., 2023; Rajkumar et al., 2022; Al-nayili et al.,2023; Portia et al., 2020; Xavier et al., 2020).

Supercapacitors (SCs), address several of these challenges due to their high-power density, rapid charge-discharge capability, long cycle life, and stability. They have been widely implemented in electric vehicles, renewable energy systems, portable electronics, and industrial power backup applications (Conway et al., 2013; Alex et al., 2021; Angelin et al., 2022; Al-Abidy et al., 2023).

Electrochemical supercapacitors operate primarily through two mechanisms: electric double-layer capacitance (EDLCs), which depends on ion adsorption at the electrode-electrolyte interface, and

pseudocapacitance, which relies on fast, reversible faradaic reactions (Chun et al., 2015; Al-Nayili et al., 2021). Carbon-based materials (Kumar et al.,2024; Kumar et al., 2023) typically utilize high surface area, porous carbon materials such as activated carbon, carbon nanotubes, and graphene, dominate EDLC applications (Cao et al., 2019; Zheng et al., 2014; Korkmaz et al., 2020; Ajel et al., 2022; Alwan et al., 2022). Conversely, pseudocapacitors rely on redox reactions or electron transfer (faradaic reactions) for charge storage, often incorporating conductive polymers, metals, and transition metal oxides (Mohammadnia et al., 2020; Yue et al., 2022).

Despite the potential of SCs, challenges remain in their widespread commercial adoption, particularly in the case of pure carbon nanomaterials. The low capacitance and energy density of these materials have hindered their extensive use in energy storage applications. To overcome these limitations, researchers are exploring various strategies, including the development of novel electrolytes and the optimization of electrode materials and structures, such as hybrid systems that combine the advantages of both EDLCs and pseudocapacitors (Chandra Sekhar et al., 2022; Yadav, 2020; Mangiri et al., 2025). In recognition of their intriguing electrochemical characteristics (Kumar et al., 2025; Bogale et al., 2025), metal oxides have been synthesized and studied using a variety of synthetic techniques for electrochemical capacitors (Yadav 2020; Chmiola et al. 2006; Balakrishnan et al., 2014; Sharma et al., 2025). Some of these materials are considered feasible due to their multiple oxidation states and double-layer charge storage capabilities, making them suitable alternatives to carbon-based materials for the supercapacitor applications (Balakrishna et al., 2014; Chmiola et al., 2006).

Recent studies have been focused on significant advancements in emerging electrode materials for high-performance energy storage. Mangiri et al. (2025) systematically analyzed M5X4 MXenes, emphasizing their unique stoichiometry, exceptional electrical conductivity, and adaptable surface chemistry, which enable efficient ion intercalation and pseudocapacitive behavior for enhanced energy and power densities. Khan et al. (2025) focused on transition metal dichalcogenides (TMDCs) noting their tunable morphology, high surface area, and strong redox activity that position them as promising candidates for next-generation supercapacitors. Ramachandran et al. (2025) reviewed recent progress in black phosphorus, underscoring its favorable electrochemical properties and potential integration into future sustainable energy-stroage technologies. At present, research is also progressing to find alternatives to costly and toxic materials that possess lower specific surface areas and limited porosity (Balakrishnan et al., 2014). Electrode materials prepared from transition metal oxides offer advantages such as environmental friendliness and easy availability. Several metal oxides, such as RuO_2, NiOx, IrO_2, Co_3O4, CoO, and MgO_2 have been found suitable for achieving higher capacitance, and stability (Bi et al., 2010; Yoon et al., 2001; Kim et al., 2013; Chen et al., 2011; Wang et al., 2014; Zhang et al., 2014; Rajeshwari et al., 2009). However, the widespread use of RuO_2-despite its exceptional reversibility, high specific capacitance, and long-life cycle is limited due to its high cost, toxicity, low specific surface area, restricted porosity, and the use of toxic precursors (Balakrishnan et al., 2014; Yoon et al., 2001). Therefore, researchers are focusing on cost-effective, environmentally benign, nontoxic and readily accessible alternatives (Kumar et al., 2025; Verma et al., 2025; Devi et al., 2024). Copper oxide (CuO) offers advantage such as abundance, ease of synthesis, low toxicity, and favorable electrocatalytic properties, along with diverse morphologies (Zaidan et al., 2019; Gbair et al., 2022). Shinde et al., (2016), reported the application of CuO in the fabrication of high-performance electrode material for supercapacitors. In addition, considerable research has demonstrated that doping magnesium oxide (MgO) with suitable additives can significantly improve supercapacitor performance.

Our proposed work focuses on developing a cost-effective MgO-based electrode material with significantly improved supercapacitive performance through the integration of CuO nanoparticles. The CuO-NPs were synthesized through a simple scalable method, and their incorporation into MgO enabled enhanced charge storage capability, improved electrical conductivity, and superior physicochemical characteristics. The MgO/CuO hybrid material was thoroughly characterized and demonstrated excellent electrochemical efficiency, validating the effectiveness of metal-metal oxide hybridization strategies report in recent literature (Thakur & Thakur, 2025; Balkrishna et al., 2024; Kumar et al., 2024; Verma et al., 2024).

2. MATERIALS AND METHODS

The chemicals $Cu(NO_3)_2.3H_2O$ (copper nitrate), NaOH (sodium hydroxide), C_2H_5OH (ethanol),

 https://doi.org/10.37819/nanofab.2025.0008

MgO (magnesium oxide) powder, carbon black, NMP (N-Methyl-2-pyrrolidone), and PVDF (polyvinylidene fluoride) were of AR grade and used without further purification (Table 1).

To obtain the precipitate of CuO-NPs, a 0.1M solution of $Cu(NO_3)_2.3H_2O$ was stirred on a magnetic stirrer for 30 minutes, followed by the dropwise addition of 0.1 M NaOH. This mixture was stirred for an additional 45 minutes. The CuO-NPs were separated using centrifugation, washed with a 5 % ethanolic solution, and dried at 75^0C for 5 hours in a hot air oven. The dried CuO-NPs were then calcined at 300^0C for 3 hours in the furnace.

For the synthesis of the MgO/CuO composite, 100 mg of CuO-NPs was dispersed in 100 mL of double-distilled water (DDW) and stirred for 2 hours, followed by 3 hours of sonication. MgO precursor powder was then added, and the mixture was stirred further to obtain a homogeneous suspension. Finally, the mixture was dried in a controlled oven environment to obtain the MgO/CuO composite powder (Figure 1). The yield of CuO/MgO was found 100%.

3. Characterization of Mgo/Cuo

3.1 SEM and EDX Analysis

The morphological characteristics of MgO, CuO-NPs and the MgO/CuO composite were investigated using Scanning Electron Microscopy (SEM), and the corresponding images were presented in Figure 2. A Zeiss EVO 18 microscope was used for the SEM analysis.

The SEM image of MgO reveals irregularly shaped particles with an asymmetric morphology, indicating a relatively rough and non-uniform particle distribution. which is consistent with previously reported morphologies of MgO powders that typically exhibit aggregated and irregular particles (Sim et al., 2024; Proniewicz et al., 2024).

The SEM images of CuO-NPs clearly show spheroidal particles, which are characteristic of well-formed CuO-NPs. Similar spherical or quasispherical CuO nanostructures have been widely reported in literature for nano particles synthesized via, sol gel, chemical precipitation and green chemistry approaches (Taghavi 2018). The morphology suggests the formation of NPs with relatively uniform shape and size. The SEM image of the MgO/CuO composite exhibits a semispherical morphology, indicating a significant change in particle structure upon the incorporation of CuO with MgO. This morphological transformation may enhance the functional properties of the composite, making it beneficial for various applications.

The elemental composition of the synthesized materials was confirmed using energy-dispersive X-ray spectroscopy (EDX) with an AMETEK system (Hoang et al., 2019). The EDX spectrum of MgO powder (Figure 3) shows a clear dominance of magnesium (Mg) and oxygen (O), consistent with the expected composition of MgO. The weight and atomic percentage of Mg and O were found to be 47.5 % (42.2%) and 52.5 % (57.8%) respectively. The elemental analysis of CuO-NPs confirmed the presence of copper (Cu) and oxygen (O), with weight

Table 1. List of chemicals used in the present study along with their purity, grade and supplier details

Chemical	Formula/ abbreviation	Purity	Grade	Company
Copper nitrate	$Cu(NO_3)_2.3H_2O$	≥99%	AR	Merck
Sodium hydroxide	NaOH	≥98%	AR	Merck
Ethanol	C_2H_5OH	≥99.9% (Absolute)	AR	Merck
Magnesium oxide	MgO	≥99%	AR/HPLC	Merck
N-Methyl-2-pyrrolidone	NMP	≥99.5%	AR	Merck
Polyvinylidene fluoride	PVDF	≥99%	AR/Battery grade	Sigma-Aldrich

and atomic percentages of 72.5 % (59.7%) and 27.5 % (40.3%), respectively, which align with the expected 1:1 atomic ratio of Cu to O in CuO. In the MgO/CuO composite, the weight and atomic percentages of Cu, Mg, O, and C, were determined to 40.7 % (22.1 %), 26.6% (19.9%), 28.7% (49.7%) and 4% (8.3%) respectively. A small peak at~ 2.2. keV corresponds to Au sputter-coating used to prevent charging during SEM imaging.

3.2. FTIR Analysis

The Fourier Transform Infrared (FTIR) spectra of bulk MgO, CuO-NPs and their MgO/CuO composite were analyzed using a Thermo Scientific Nicolet iS5 spectrometer (with iD1 ATR module) to study the functional group and bonding interactions (Figure 4(a)). The FTIR spectrum of bulk MgO shows prominent peaks at 3697 cm^{-1}, 2418 cm^{-1}, 1592 $^{-1}$, and 620 cm^{-1}. The peak at 3697 cm^{-1} is attributed to the stretching vibrations of hydroxyl groups, indicating the presence of surface-bound water or hydroxylation of MgO surface, consistent with earlier reports for MgO materials (Kulkarni et al., 2017; Sembiring et al., 2017). The absorption at 2418 cm^{-1} can be linked to the stretching vibrations of the C=O bond, possibly due to absorption of atmospheric carbon dioxide, which is also commonly observed and other alkaline oxides (Kulkarni et al., 2017). The peak at 620 cm^{-1} is characteristic of Mg-O stretching vibration, confirming the presence of magnesium oxide framework (Sembiring et al., 2017; Essien et al., 2020). The FTIR spectrum of CuO-NPs shows significant peaks at 3562 cm^{-1}, 1598 cm^{-1}, 1383 cm^{-1}, 733 cm^{-1} and 602 cm^{-1}. The peak at 733 cm^{-1} is indicative of Cu-O stretching confirming the presence of copper oxide in nanoparticle form. The sharp peak at 602 cm^{-1} is also associated with Cu-O stretching mode, further supporting the formation of CuO-NPs (Panesar et al., 2020; Gouda et al., 2023; Topal Canbaz, 2023; Vinayagar et al., 2024).

The FTIR spectrum of the MgO/CuO composite displays peaks at 3687 cm^{-1}, 1596 cm^{-1}, 988 cm^{-1}, 872 cm^{-1} and 614 cm^{-1}. The presence of peaks at 988 cm^{-1} and 872 cm^{-1} indicate interaction between the MgO and CuO phases, possibly involving the formation of magnesium–copper oxide linkage or surface interaction between the two oxides or surface interaction altering the oxygen environment between these two oxides (Muhaymin et al. 2024). Similar new vibration bands arising from metal-oxygen linkage in mixed oxides have been reported in literature (Gouda et al., 2023). The peak at 614 cm^{-1} is associated with Cu-O stretching vibration, characteristic of the CuO phase, and further supports the successful incorporation of CuO into MgO matrix (Gouda et al., 2023).

The spectral features of all three samples showed good agreement with reported FTIR data of MgO and CuO, and mixed metal oxide systems, supporting the successful formation and interaction of the composite.

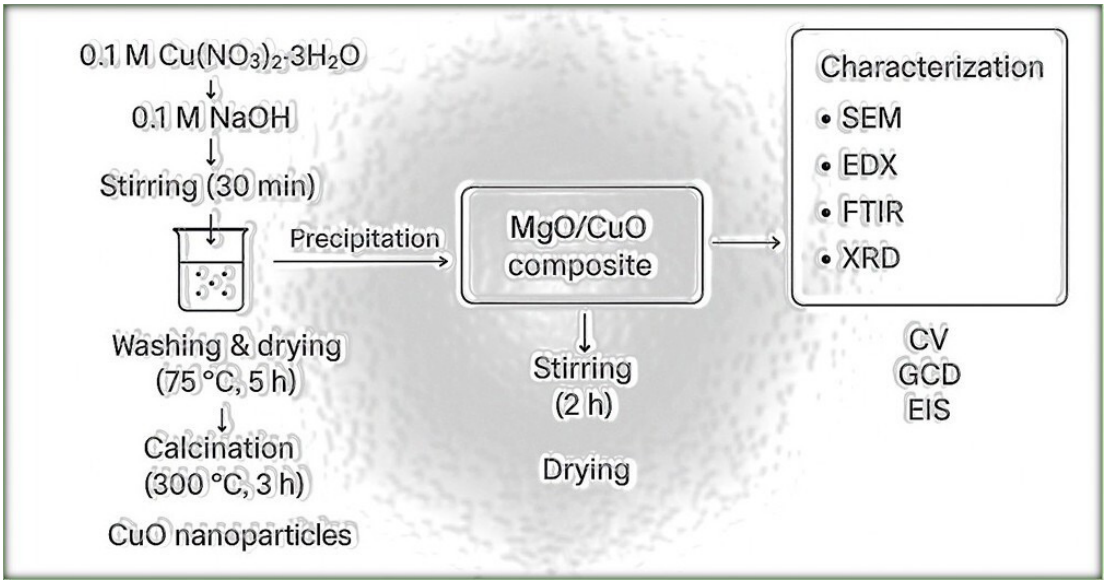


Figure 1. Schematic representation of the synthesis process of the CuO/MgO composite

 https://doi.org/10.37819/nanofab.2025.0008

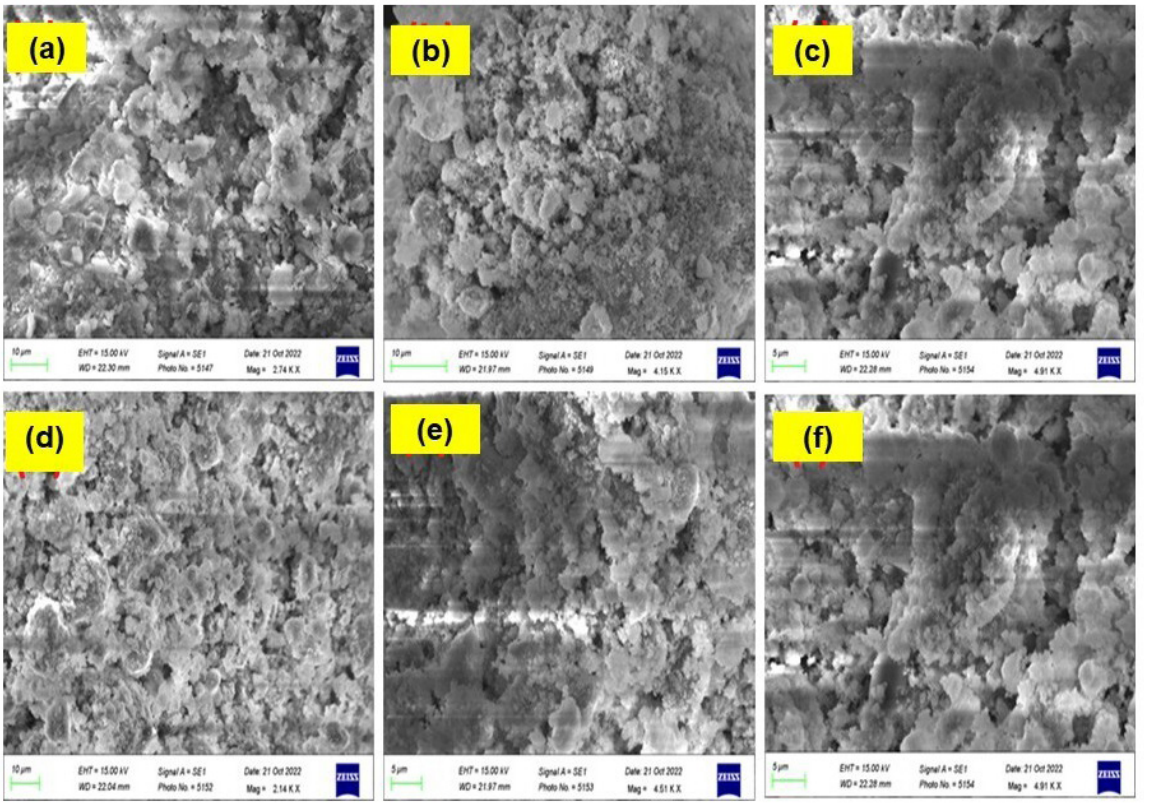


Figure 2. SEM micrographs showing the morphology of (a) bulk MgO, (b) CuO-NPs, and (c-f) the MgO/CuO composite

3.3. XRD Analysis

X-ray diffraction (XRD) analysis was performed using a Rigaku SmartLab SE diffractometer to determine the crystal structure of the CuO-NPs and the MgO/CuO composite. Figure 3(b) shows the XRD patterns of the CuO-NPs and the MgO/CuO composite and indicates the semicrystalline nature of the CuO-NPs. Which is consistent with literature where nanoparticles synthesized via wet-chemical, sol gel methods or precipitation methods often show similar broadening due to nanoscale grain size (Jillani, S., 2018; Mizoshiri, M. & Yoshidomi, K. 2021). The observed peaks at $2\theta = 32.5^0$, 35.6^0, 38.6^0, 48.6^0, 53.4^0, 65.9^0, and 67.8^0 are indexed to the (110), (002), (111), (-202), (020), (-311), and (220) planes, respectively, which are consistent with monoclinic structure of CuO (JCPDS No 48-1548). These peak positions and planes are in agreement with previously reported diffraction patterns for nanoscale monoclinic CuO confirming the successful formation of CuO-NPs (Karthikeyan, B., 2021; Kalaiyarasi, M., 2024).

In contrast the XRD pattern of the MgO/CuO composite shows a noticeable reduction in peak intensity and broadening, particularly in the region corresponding to CuO, indicating a shift towards an amorphous like character. The reduction in peak intensity and broadening observed in CuO region of Mgo/CuO composite's XRD pattern can be attributed to lattice disruption caused by MgO incorporation which disturbs the crystalline order of CuO, consistent with known phenomena in mixed metal oxide nano composites (Sundeep, D., 2016)

The composite also displays additional peaks at 2θ values of 42.7^0 and 56.1^0, corresponds to the (200) and (220) planes, respectively, which are typically associated with the cubic structure of MgO (JCPDS No 45-0946). The particle sizes of CuO and the MgO/CuO composite were calculated to be 12.18 nm and 8.57 nm respectively (Wang, 2021).

4. ELECTROCHEMICAL STUDY

Electrochemical measurements were performed using a Biologic VSP-3e potentiostat. The composite materials were mixed with PVDF, carbon black, and NMP (80:10:10) to prepare the electrode slurry, which was coated onto precleaned graphite foam and

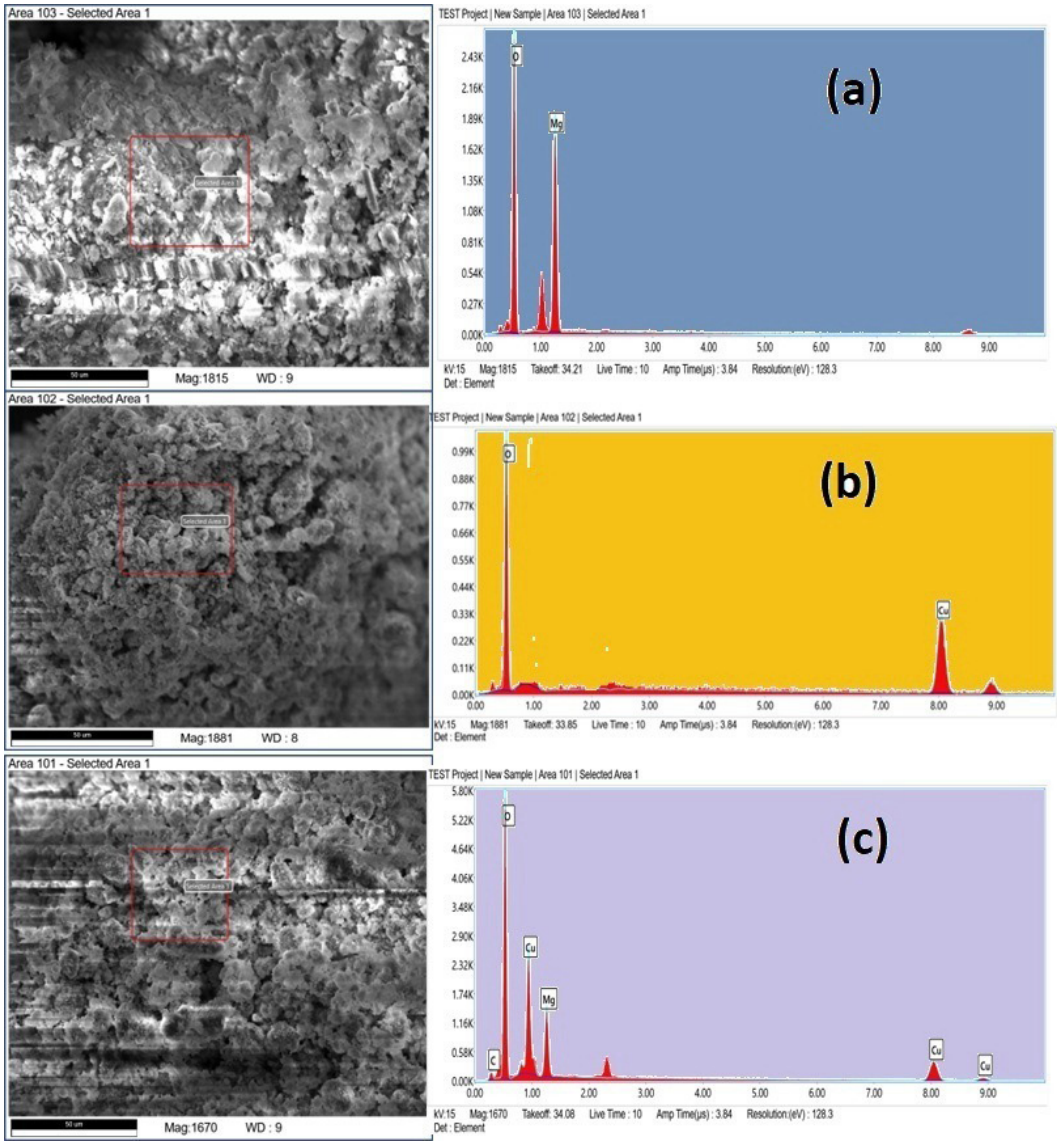


Figure 3. EDX spectra of (a) bulk MgO, (b) CuO-NPs, and (c) the MgO/CuO composite dried at 80^0C for 10 h.

The mass difference before and after coating confirmed an active material loading of~ 1mg. The Ni foam, Ag/AgCl, and platinum wire served as the working, reference, and counter electrodes, respectively, in 1M KOH. Cyclic voltammetry (CV), Galvanostatic charge-discharge (GCD), cycling stability, and Electrochemical impedance spectroscopy (EIS) analysis were conducted (Balasubramanian et al., 2015; Li et al., 2014).

4.1. CV Analysis

At scan rates of 10mV/s, 20mV/s, 30mV/s, 50mV/s, 75mV/s, and 100mV/s, CV curves were obtained within the potential window of 0.2 to 0.8 V, as shown in Figure 5 (a-f). For MgO, the specific capacitance values were found to be 2411.31 F/g, 665.78 F/g, 366.47 F/g, 185.44 F/g, 89.98 F/g, and 67.49 F/g, respectively. For CuO, the specific capacitance values were 3014.61 F/g, 779.37 F/g, 438.17 F/g, 228.55 F/g, 144.55 F/g, and 108.41 F/g, respectively.

For the MgO/CuO composite in the three-electrode configuration, the specific capacitance values were significantly enhanced and measured to be 5750.66 F/g, 1718.12 F/g, 904.79 F/g, 442.82 F/g, 202.28 F/g, and 151.71 F/g, respectively. However, in the two-electrode configuration, the composite exhibited

 https://doi.org/10.37819/nanofab.2025.0008

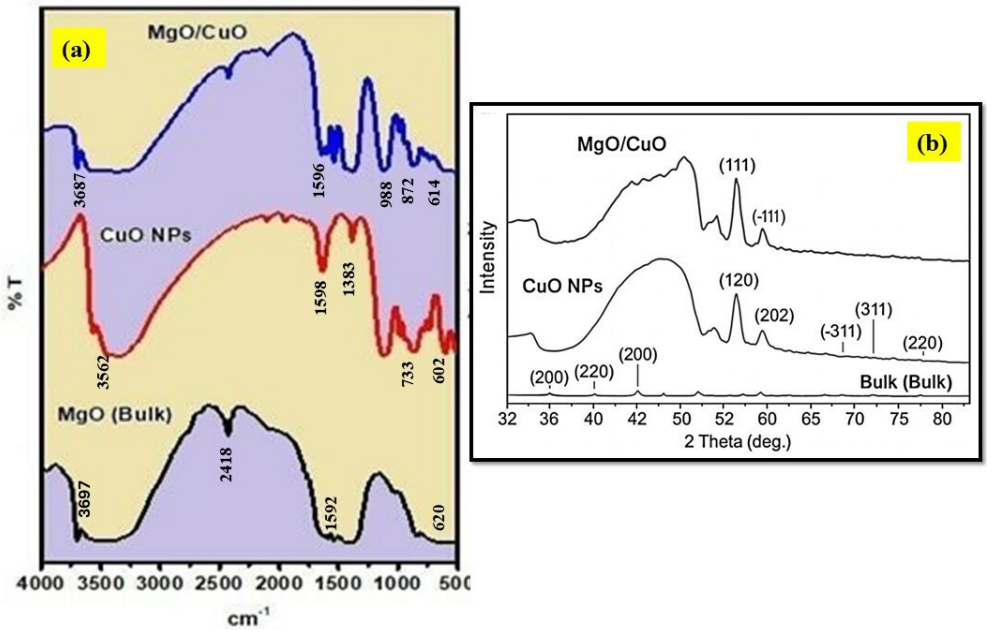


Figure 4. (a) FTIR spectra of bulk MgO, CuO-NPs, and MgO/CuO composite. (b) XRD patterns of CuO-NPs and the MgO/CuO composite

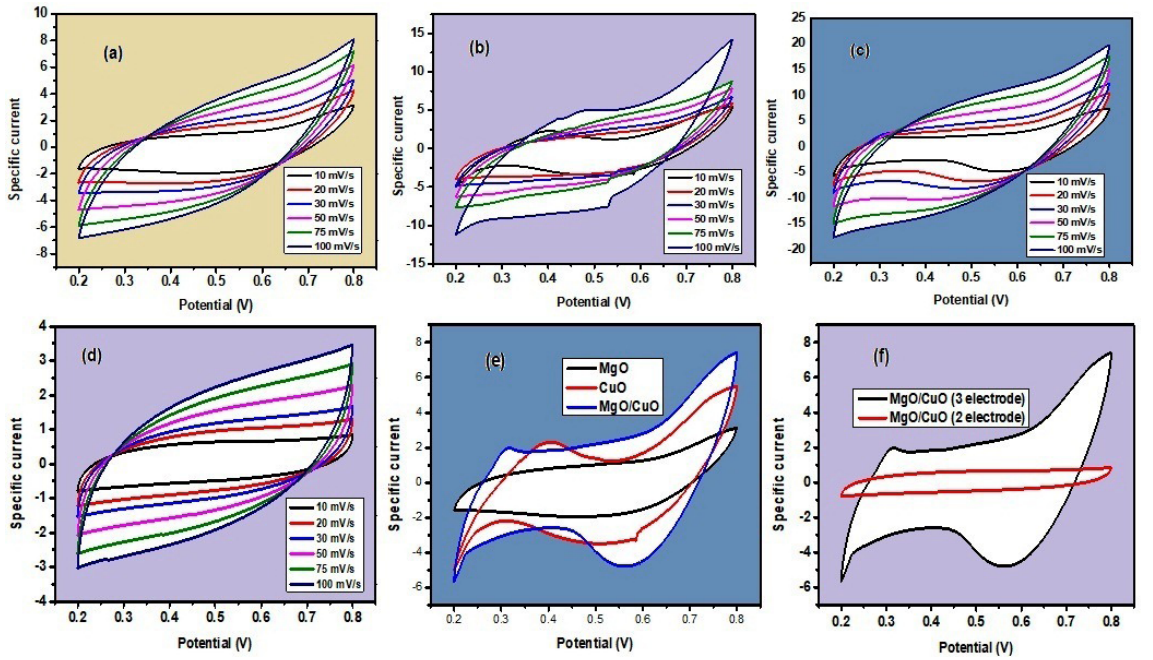


Figure 5. CV curves recorded at different scan rates for (a) bulk MgO (b) CuO-NPs (c) MgO/CuO (three-electrode configuration), (d) MgO/CuO (two-electrode configuration) (e) comparison of MgO, CuO-NPs, and MgO/CuO in a three-electrode setup, and (f) comparison of MgO/CuO performance under two-and three-electrode systems specific capacitance values of 1135.72 F/g, 351.54 F/g, 177.52 F/g, 85.60 F/g, 37.95 F/g, and 28.46 F/g, respectively.

The quasi-rectangular CV curves of the composite indicate significant energy storage capability and good material stability of the particular materials. These results also show that specific capacitance decreases with increasing scan rate due to the limited diffusion of charge carriers during the charge storage process (Gajraj et al., 2021). The decrease in specific capacitance suggests that ion diffusion plays a dominant role in the charge storage mechanism. Al lower scan rates, the electrolyte ions have sufficient time to penetrate deeply into the porous structure of the electrode, resulting in higher specific capacitance (Rastogi et al., 2024). A similar trend in specific capacitance has also been reported by Devi et al. (2022) for synthetically prepared Ag/r-GO nanocomposites.

4.2. GCD Analysis

The GCD curves of MgO, CuO-NPs, and MgO/CuO under three and two-electrode systems at different current densities (2, 4, 6, 8, 10, and 12 A/g) are presented in Figure 6. MgO exhibited specific capacitance values of 113.3, 57.7, 40, 35.5, 33.3, and 13.3 F/g (Figure 6(a)), whereas CuO-NPs showed values of 240, 66.6, 60, 53.3, 44.4, and 26.6 F/g at the same current densities (Figure 6(b)) (Ramachandran et al., 2024). Based on three-electrode measurements, the specific capacitance of the MgO/CuO composite was found to be 444.4, 288.8, 213.3, 168.8, 133.3, and 40 F/g (Figure 6(c)) (Durga et al., 2024). A comparison of MgO/CuO with other electrode materials is shown in Table 2.

Figure 6(d) presents the symmetrical triangular GCD curve pattern of MgO/CuO in the two-electrode setup. These curves indicate high electrochemical reversibility, characteristics of efficient SCs (Wei et al., 2016). At current densities of 2, 4, 6, 8, 10, and 12 A/g, the specific capacitance values were 35.5, 33.3, 26.6, 17.7, 11.1, and 6.6 F/g respectively.

The specific capacitance decreases with increasing current density due to diffusion-controlled charge storage, consistent with Liu et al. (2020), who observed a similar trend for r-GO/polypyrrole GCD.

The cyclic stability analysis was performed for 5000 cycles, and it was observed that after 1000 cycles (for the three-electrode setup), MgO NPs, CuO-NPs, and MgO/CuO NPs retained 99.1%, 99.7%, and 100%, of respectively. After 2000 GCD cycles, the retention values were 94.2%, 96.2%, and 100%, respectively. After 4000 GCD cycles, the capacitance retention decreased to 83.2%, 85.8%, and 96.8% respectively. After 5000 GCD cycles, MgO, CuO, and MgO/CuO retained 82.7%, 84.9%, and 96.8%

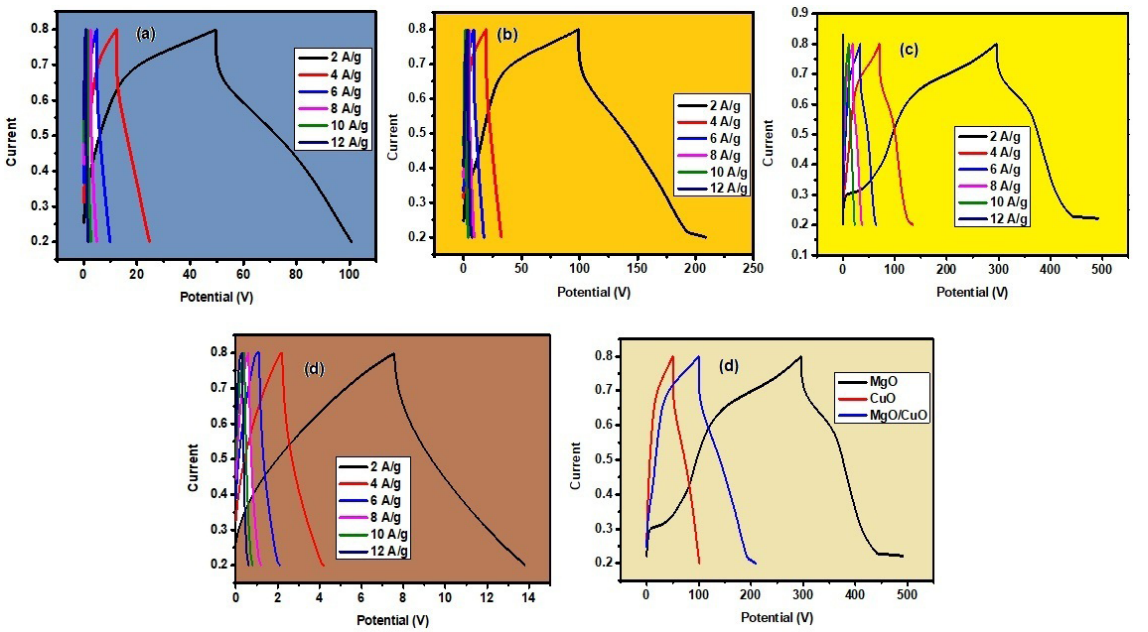


Figure 6. GCD cures at different current densities for (a) bulk MgO, (b) CuO-NPs, (c) MgO/CuO (three-electrode configuration), (d) MgO/CuO (two-electrode configuration), and (e) comparison of GCD behavior of MgO, CuO-NPs, and MgO/CuO in the three-electrode setup

 https://doi.org/10.37819/nanofab.2025.0008

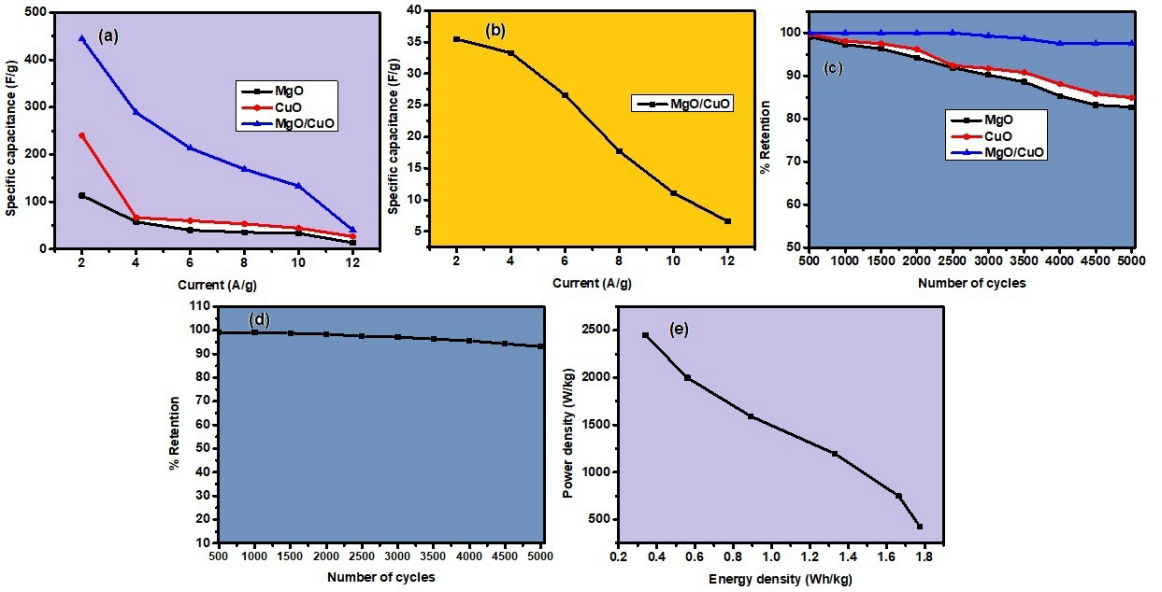


Figure 7. Variation of specific capacitance with current density for (a) three-electrode configuration and (b) two-electrode configuration. (c) cyclic stability and percentage capacitance retention for MgO, CuO-NPs, and MgO/CuO (three-electrode setup) (d) cyclic stability of MgO/CuO in a two-electrode setup, and (e) Ragone plot showing the relationship between power density and energy density

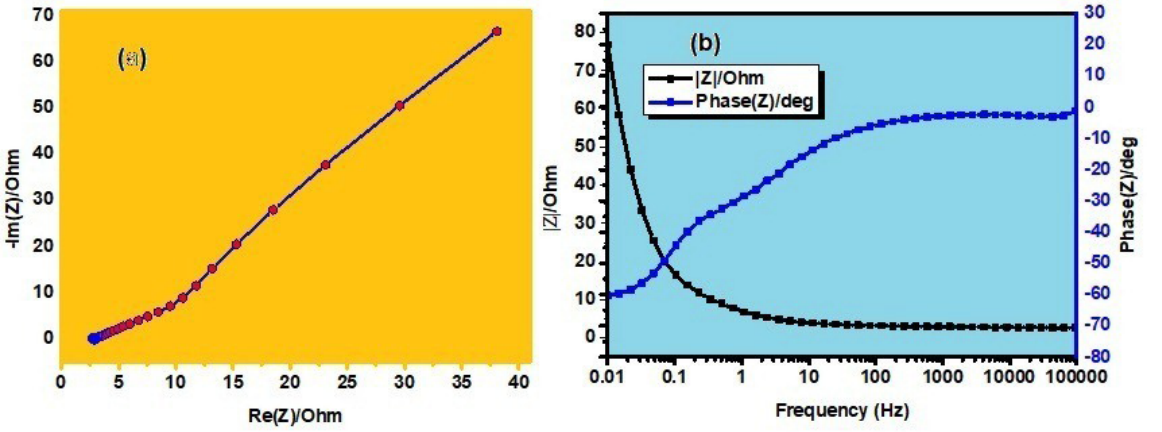


Figure 8. (a) Nyquist plot of the MgO/CuO composite, (b) Bode plot showing the phase angle variation with frequency

of their initial capacitance respectively (Figure 7 (c)). For the two-electrode setup, the MgO/CuO composite retained 93.1% of its initial capacitance after 5000 GCD cycles (Figure 7 (d)). Capacitance degradation during cycling arises from repeated ion insertion-extraction, limiting practical use (Kim et al., (2022)), similar to trends reported by Kumari et al. (2017) for MnO2/r-GO.

SCs bridge the gap between high-power/low-energy capacitors and rechargeable batteries. The power densities of MgO/CuO were found to be 426, 749.2, 1197, 1593, 1998, and 2448 W/kg at corresponding energy densities of 1.775, 1.665, 1.33, 0.89, 0.56, and 0.34 Wh/kg (Figure 7 (e)).

4.3. EIS Analysis

The impedance characteristics of the MgO/CuO composite were investigated using the Nyquist plot (Figure 8 (a)). The absence of a semicircle in the high-frequency region indicates negligible charge-transfer resistance from the electrolyte, while the straight line in the low- frequency region suggests excellent ion-diffusion behavior within the composite. The Bode

Table 2. Specific capacitance values of other metal oxide composites under various electrolytes and test conditions

Composites	Electrolyte	Test conditions	Specific capacitance (F/g)	References
Cu MOF/rGO	PVA-Na_2SO_4	1 A/g	385	Srimuk, P. et al., 2015
Cu MOF/rGO	0.1 M PBS	1.6 A/g	685.33	Saraf, M. et al., 2016
CuO/NCNO	1 M KOH	1 A/g	441.25	Sohouli, E., et al., 2023
Zn/SnO_2	1 M KCl	1 A/g	635	De Adhikari, A., et al., 2018
ZnO/CoS_2/NF	3 M KOH	1 A/g	400.2	Durga, I. K., et al., 2021
MgO/CuO	1 M KOH	2 A/g	444.4	Present study

plot (Figure 8 (b)), represents the variation of phase shift between voltage and current.

Nyquist plot analysis revealed an R(CR)(QR)(CR) equivalent circuit with series resistance and charge-transfer resistance values of 2.932Ω, and $7.95x10^{-17}$Ω, respectively. These values indicate good electrical conductivity of the MgO/CuO composite. Furthermore, the low Warburg impedance value ($1.55x10^{-3}$Ω) demonstrates excellent ion-diffusion capability within the MgO/CuO composite (Shinde et al., 2017).

5. CONCLUSION

The structural, morphological, and electrochemical analysis collectively confirm the successful formation of the MgO/CuO composite and its enhanced suitability as an efficient supercapacitor electrode material. FTIR and EDX analysis verified the chemical interaction and incorporation of CuO within the MgO matrix, while SEM images revealed substantial morphological refinement due to CuO addition. XRD patterns indicated a partial loss of CuO crystallinity, contributing to improved electrochemical behavior. The MgO/CuO composite demonstrated significantly higher specific capacitance, excellent rate capability, and superior cycling stability, retaining 96.8% capacitance after 5000 GCD cycles. The low resistance, fast ion diffusion, and favorable charge-transfer kinetics observed in EIS further support its enhanced performance. These findings highlight MgO/CuO as a promising, low-cost, and environmentally benign electrode material capable of bridging the performance gap between conventional capacitors and rechargeable batteries for next-generation energy storage applications.

Beyond energy storage, the findings of this study also indicate the potential applicability of MgO/CuO hybrid materials in biomedical fields. Both MgO and CuO are recognized for their biocompatibility, antimicrobial activity, and catalytic surface behavior, making them promising candidates for multifunctional biomedical platforms. The improved surface activity, high stability, and nanostructured features of the MgO/CuO composite could be exploited for antibacterial coatings, biosensing electrodes, drug-delivery carriers, and tissue-engineering scaffolds. Its enhanced electrochemical responsiveness may also contribute to improved sensing performance in biomedical diagnostics. Future investigations involving cytoxicity assessment, antimicrobial efficacy, and biological interfacing are essential to translate these material advantages into practical biomedical applications.

STATEMENTS AND DECLARATIONS

Data availability

All data are presented in this study. The authors declare no conflict of interest.

FUNDING

Not applicable.

REFERENCES

Ajel, M. K. & Al-Nayili, A. (2022). Synthesis, characterization of Ag-WO3/bentonite nanocomposites and their application in photocatalytic degradation of humic acid in water. *Environ. Sci. Pollut. Res.* https:// doi. org/ 10. 1007/ s11356- 022- 23614-4

Al-Abidy, M. & Al-Nayili, A. (2023). Enhancement of photocatalytic activities of ZnFe2O4 composite by incorporating halloysite nanotubes for effective elimination of aqueous organic pollutants. *Environ. Monit. Assess.* 195, 190. https://doi.org/10.1007/s10661-022-10811-4

Alex, J., Rajkumar, S., PrincyMerlin, J., Aravind, A., Sajan, D., & Praveen, C. S. (2021). Single step auto-igniting combustion technique grown CeO2 and Ni-doped CeO2 nanostructures for multifunctional applications. Journal of Alloys and Compounds, 882, 160409. https://doi.org/10.1016/j.jallcom.2021.160409

Al-Nayili, A. & Albdiry, M. (2021). Identification of active structure and catalytic efficiency of MCM-22 zeolite detemplated by two differentprocesses. *J. Porous Mater.* 28, 1439–1448. https://doi.org/10.1007/s10934-021-01098-w

Al-nayili, A. & Muhammad, N. J. (2023). Perovskite's LaNiMnO6/montmorillonite K10 nanocomposites: Synthesis and enhanced photocatalytic activity. *Mater. Sci. Semicond. Process.* 155, 107254. https://doi.org/10.1016/j.mssp.2022.107254

Alwan, S. H., Salem, K. H. & Alshamsi, H. A. (2022). Visible light-driven photocatalytic degradation of Rhodamine B dye onto TiO2/rGO nanocomposites. *Mater. Today Commun.* 33, 104558. https://doi.org/10.1016/j.mtcomm.2022.104558

Angelin, M. D., Rajkumar, S., Ravichandran, A. & Merlin, J. P. (2022). Systematic investigation on the electrochemical performance ofCd-doped ZnO as electrode material for energy storage devices. *J. Phys. Chem. Solids* 161, 110486. https://doi.org/10.1016/j.jpcs.2021.110486

Balakrishnan, A., Subramanian K.R.V. (2014). Nanostructured ceramic oxides for supercapacitor applications. CRC Press,Boca Raton. https://www.routledge.com/Nanostructured-Ceramic-Oxides-for-Supercapacitor-Applications/Balakrishnan-Subramanian/ p/ book/9781138072671? srsltid=AfmBOorBqA4Fuv4KCEPs RW0rI SloA3e0OAx4h Ylo Ok 2Ha AqsUuYVD4Kk

Balasubramanian, S. & Purushothaman, K.K. (2015). Carbon coated flowery V2O5 nanostructure as a novel electrode material for high-performance supercapacitors. Electrochim. Acta, 186 285–291. https://doi.org/ 10.1016/j.electacta.2015.10.160.

Balkrishna, A., Thakur, N., Patial, B., Sharma, S., Kumar, A., Arya, V., & Amarowicz, R. (2023). Synthesis, characterization and antibacterial efficacy of Catharanthus roseus and Ocimum tenuiflorum-mediated silver nanoparticles: phytonanotechnology in disease management. *Processes*, *11*(5), 1479.

Bi, R. R., Wu, X. L., Cao, F. F., Jiang, L. Y., Guo, Y. G., & Wan, L. J. (2010). Highly dispersed RuO2 nanoparticles on carbon nanotubes: facile synthesis and enhanced supercapacitance performance. The Journal of Physical Chemistry C, 114(6), 2448-2451. https://doi.org/10.1021/jp9116563

Bogale, A. M., Ramachandran, T., Suk, M. E., Badassa, B. B., Solomon, M. M., He, J., ... & Tesema, F. B. (2025). Boosted Charge Storage in Symmetric Supercapacitors Using Zn-Co/MgCo2O4 Hybrid Nanosheets. *Journal of Physics and Chemistry of Solids*, 113079. https://doi.org/10.1016/j.jpcs.2025.113079

Cao, C., Zhou, Y., Ubnoske, S., Zang, J., Cao, Y., Henry, P., & Glass, J. T. (2019). Highly stretchable supercapacitors via crumpled vertically aligned carbon nanotube forests. Advanced Energy Materials, 9(22), 1900618. https://doi.org/10.1002/aenm.201900618

Chandra Sekhar, S., Ramulu, B., & Yu, J. S. (2022). Transition metal oxides for supercapacitors. In Nanostructured Materials for Supercapacitors (pp. 267-292). Cham: Springer International Publishing. https://www.researchgate.net/publication/360711820_Transition_Metal_Oxides_for_Supercapacitors

Chen, Y. M., Cai, J. H., Huang, Y. S., Lee, K. Y., & Tsai, D. S. (2011). Preparation and characterization of iridium dioxide–carbon nanotube nanocomposites for supercapacitors. Nanotechnology, 22(11), 115706. https://doi.org/10.1088/0957-4484/22/11/115706

Chmiola, J., Yushin, G., Gogotsi, Y., Portet, C., Simon, P., & Taberna, P. L. (2006). Anomalous increase in carbon capacitance at pore sizes less than 1 nanometer. Science, 313(5794), 1760-1763. https://doi.org/10.1126/science.1132195

Chun, S. E., Evanko, B., Wang, X., Vonlanthen, D., Ji, X., Stucky, G. D., & Boettcher, S. W. (2015). Design of aqueous redox-enhanced electrochemical capacitors with high specific energies and slow self-discharge. Nature communications, 6(1), 7818. https://doi.org/10.1038/ncomms8818

Conway, B. E. (2013). Electrochemical supercapacitors: scientific fundamentals and technological applications. Springer Science & Business Media. https://link.springer.com/book/10.1007/978-1-4757-3058-6

De Adhikari, A., Oraon, R., Tiwari, S. K., Saren, P., Maity, C. K., Lee, J. H. & Nayak, G. C. (2018). Zn-doped SnO 2 nano-urchin-enriched 3D carbonaceous framework for supercapacitor application. New Journal of Chemistry, 42(2), 955-963. https://doi.org/10.1039/C7NJ03792A

Devi, M., Sharma, S., Kumar, P., Thakur, N., Kumar, G., Sharma, M. V., Jeet, K., & Thakur, N. (2024). Antifungal, antibacterial and antioxidant activity of Pinus roxburghii mediated green synthesized zinc and gadolinium doped manganese oxide nanoparticles. *Colloids and Surfaces C: Environmental Aspects*, *2*, 100046.

Devi, N. R., Sinha, S., Singh, W., Nongthombam, S. & Swain, B.P. (2022). Silver-decorated reduced graphene oxide nanocomposite for supercapacitor electrode application, Bull. Mater. Sci. 45, 1-11. https://doi.org/10.1007/s12034-021-02583-3

Durga, I. K., Raghavendra, K. V. G., Kundakarla, N. B., Alapati, S., Ahn, J. W., & Srinivasa Rao, S. (2021). Facile synthesis of coral reef-like ZnO/CoS2 nanostructure on nickel foam as an advanced electrode material for high-performance supercapacitors. Energies, 14(16), 4925. https://doi.org/10.3390/en14164925

Durga, I. K., Roy, N., Ramachandran, T., Kumar, K. D., Ansar, S., Kumar, Y. A., ... & Joo, S. W. (2024). Innovative synthesis strategies for Rambutan-shaped CuNiO2 electrodes in high-performance supercapacitors. Journal of Physics and Chemistry of Solids, 192, 112117. https://doi.org/10.1016/j.jpcs.2024.112117

Essien, E. R., Atasie, V. N., Oyebanji, T. O., & Nwude, D. O. (2020). Biomimetic synthesis of magnesium oxide nanoparticles using Chromolaena odorata (L.) leaf extract. Chemical Papers, 74, 2101-2109. https://doi.org/10.1007/s11696-020-01056-x

Gajraj, V., & Mariappan, C.R. (2021). CuWO4: A promising multifunctional electrode material for energy storage as in redox active solid-state asymmetric supercapacitor and an electrocatalyst for energy conversion in methanol electro-oxidation, J. Electroanal. Chem. 895, 115504. https://doi.org/10.1016/j.jelechem.2021.115504.

Gbair, G. A. & Alshamsi, H. A. (2022). Facile green synthesis of CuO-ZnO nanocomposites from *Argyreia nervosa* leaves extract forphotocatalytic degradation of Rhodamine B dye. *Biomass Convers. Biorefin.* https:// doi. org/ 10. 1007s/ s13399- 022- 03408-x.

Gouda, M., Almutairi, H. H., & Abd El-Lateef, H. M. (2023). Hyaluronic acid/cellulose acetate polymeric mixture containing binary metal oxide nano-hybrid as low biodegradable wound dressing. *Journal of Materials Research and Technology*, *26*, 7925–7935. https://doi.org/10.1016/j.jmrt.2023.09.086

Hoang, V.C., Dinh, K. N., & Gomes, V. G. (2019). Iodine doped composite with biomass carbon dots and reduced graphene oxide: a versatile bifunctional electrode for energy storage and oxygen reduction reaction. Journal of Materials Chemistry A, 7(39), 22650-22662. https://doi.org/10.1039/C9TA05559B

Jillani, S., Jelani, M., Ahmad, S., Hassan, N. U., & Hafeez, M. (2018). Synthesis, characterization and biological studies of copper oxide nanostructures. Materials Research Express, 5(4), 045006. https://doi.org/10.1088/2053-1591/aab864

Kalaiyarasi, M., Nivedha, M., Mani, M., Harikrishnan, R., Kumar, J. K., Loganathan, S., & Kaviyarasu, K. (2024). Synthesis of CuO/NaCuSO4 nanocomposite using an aqueous extract of Tribulus terrestris and their structural, optical, morphology and dielectric studies. Chemical Papers, 78(5), 3083–3098. https://doi.org/10.1007/s11696-023-03294-1

Karthikeyan, B. (2021). Raman spectral probed electron–phonon coupling and phonon lifetime properties of Ni-doped CuO nanoparticles. Applied Physics A, 127(3). https://doi.org/10.1007/s00339-021-04330-1

Khan, R., Kalla, R. M. N., Ramachandran, T., Al-Sehemi, A. G., Kumar, Y. A., Somu, P., & Lee, J. (2025). Transition metal dichalcogenides for next-generation supercapacitors: recent advances, challenges, and future perspectives. Journal of Alloys and Compounds, 182874. https://doi.org/10.1016/j.jallcom.2025.182874

Kim, S. B., Kumar, N., Park, S. J., & Lee, S. Y. (2022). Recent advanced supercapacitor: A review of storage mechanisms, electrode materials, modification, and perspectives. Nanomaterials, 12, 3708. https://doi.org/10.3390/nano12203708

Kim, S. I., Lee, J. S., Ahn, H. J., Song, H. K., & Jang, J. H. (2013). Facile route to an efficient NiO supercapacitor with a three-dimensional nanonetwork morphology. ACS applied materials & interfaces, 5(5), 1596-1603. https://doi.org/10.1021/am3021894

Korkmaz, S., & Kariper, İ. A. (2020). Graphene and graphene oxide-based aerogels: Synthesis, characteristics and supercapacitor applications. Journal of Energy Storage, 27, 101038. https://doi.org/10.1016/j.est.2019.101038

Kulkarni, J., Ravishankar, R., Nagabhushana, H., Anantharaju, K. S., Basavaraj, R. B., Sangeeta, M. & Renuka, L. (2017). Structural, optical and photocatalytic properties of MgO/CuO nanocomposite prepared by a solution combustion method. Materials Today: Proceedings, 4(11), 11756-11763. https://doi.org/10.1016/j.matpr.2017.09.092

Kumar A., Koyyada, Y. G., Ramachandran, T., Kim, J.-H., Sajid, S., Moniruzzaman, M., Alzahmi, S., & Obaidat, I. M. (2023). Carbon materials as a conductive skeleton for supercapacitor electrode applications: A review. Nanomaterials, 13, 1049. https://doi.org/10.3390/nano13061049

Kumar, P., Arya, V., Kumar, A., & Thakur, N. (2025). Polymer/phytochemical mediated eco-friendly synthesis of Cu/Zn doped hematite nanoparticles revealing biological properties and photocatalytic activity. *International Journal of Materials Research*, *116*(1), 30-49.

Kumar, P., Kumar, S., Tapwal, A., Nimesh, S., & Thakur, N. (2024). Water purification and biological efficacy of green synthesized Co/Zn-Doped α-Fe2O3 nanoparticles. *Sustainable Chemistry for the Environment*, *8*, 100160.

Kumar, S., Joshi, N. C., Rawat, B. S., & Gururani, P. (2024). Synthesis and electrochemical potential of CoFe2O4/Ppy-based material. Inorganic Chemistry Communications, 167, 112692. https://doi.org/10.1016/j.inoche.2024.112692.

Kumar, Y. A., Alagarasan, J. K., Ramachandran, T., Rezeq, M., Bajaber, M. A., Alalwiat, A. A., Moniruzzaman, M., & Lee, M. (2024). The landscape of energy storage: Insights into carbon electrode materials and future directions—Carbon materials as a conductive skeleton for supercapacitor electrode applications: A review. Journal of Energy Storage, 86 (Part A), 111119. https://doi.org/10.1016/j.est.2024.111119

Kumar, Y. A., Vignesh, S., Ramachandran, T., Fouda, A. M., Hegazy, H. H., Moniruzzaman, M., & Oh, T. H. (2025). Advancements in novel electrolyte materials: Pioneering the future of supercapacitive energy storage. *Journal of Industrial and Engineering Chemistry*, *145*, 191-215. https://doi.org/10.1016/j.jiec.2024.11.018

Kumari, R., Varghese, A., George, L., & Sudhakar, Y. N. (2017). Effect of solvent polarity on the photophysical properties of chalcone derivatives. RSC Advances, 7, 24204–24214. https://doi.org/10.1039/C7RA01705G

Li, H.Y., Jiao, K., Wang, L., Wei, C., Li, X. & Xie B. (2014). Micelle anchored in situ synthesis of V2O3 nanoflakes@C composites for supercapacitors. J. Mater. Chem, A2 18806–18815. https://doi.org/10.1039/C4TA04062G.

Liu, G., Shi, Y., Wang, L., Song, Y., Gao, S., Liu, D., & Fan, L. (2020). Reduced graphene oxide/polypyrrole composite: An advanced electrode for high-performance symmetric/asymmetric supercapacitor. Carbon Letters, 30, 389–397. https://doi.org/10.1007/s42823-019-00108-x

Mangiri, R., Ramachandran, T., Kumar, Y. A., Ghosh, A., Al-Sehemi, A. G., Yadav, A. K., & Mani, D. (2025). Surface engineering of M5X4 MXenes for next-gen energy solutions. Materials Today Chemistry, 48, 102864. https://doi.org/10.1016/j.mtchem.2025.102864

Mizoshiri, M., & Yoshidomi, K. (2021). Cu patterning using femtosecond laser reductive sintering of CuO nanoparticles under inert gas injection. Materials, 14(12), 3285. https://doi.org/10.3390/ma14123285

Mohammadnia, M. S., Khosrowshahi, E. M., Naghian, E., Keihan, A. H., Sohouli, E., Plonska-Brzezinska, M. E. & Ahmadi, F. (2020). Application of carbon nanoonion-NiMoO4-MnWO4 nanocomposite for modification of glassy carbon electrode: Electrochemical determination of ascorbic acid. Microchemical Journal, 159, 105470. http://dx.doi.org/10.1016/j.microc.2020.105470

Muhaymin, A., Mohamed, H. E. A., Hkiri, K., Safdar, A., Azizi, S., & Maaza, M. (2024). Green synthesis of magnesium oxide nanoparticles using Hyphaene thebaica extract and their photocatalytic activities. Scientific Reports, 14(1). https://doi.org/10.1038/s41598-024-71149-0

Naderi, L., Shahrokhian, S. & Soavi, F. (2020). Fabrication of a 2.8 V high-performance aqueous flexible fiber-shaped asymmetric microsupercapacitorbased on MnO2/PEDOT: PSS-reduced graphene oxide nanocomposite grown on carbon fiber electrode. *J. Mater.Chem. A* 8, 19588–19602. https://doi.org/10.1039/D0TA06561G

Panesar, M. J., Tchouank Tekou, C. T., Srivastava, A. K., Mohammed, J., & Kumar, P. (2020). Effect of Addition of Polyaniline (PANI) on the properties of copper (II) Oxide nanoparticles. *Journal of Physics: Conference Series*, *1531*(1), 012036. https://doi.org/10.1088/1742-6596/1531/1/012036

Portia, S., Srinivasan, R., Elaiyappillai, E., Johnson, P. M. & Ramamoorthy, K. (2020). Facile synthesis of Eu-doped CaTiO3and their enhanced supercapacitive performance. *Ionics* 26, 3543–3554. https://doi.org/10.1007/s11581-020-03494-9

Proniewicz, E., Molenda, M., Surma, O., Szkudlarek, A., & Vijayan, A. M. (2024). Plant-assisted green synthesis of MgO nanoparticles as a sustainable material for bone regeneration: Spectroscopic properties. International Journal of Molecular Sciences, 25(8), 4242. https://doi.org/10.3390/ijms25084242

Ramachandran, T., Pachamuthu, M. P., Karthikeyan, G., Hamed, F., & Rezeq, M. D. (2024). Synergistic effects in CuO/SnO2/Ti3C2Tx nanohybrids: Unveiling their potential as supercapacitor cathode material. Materials Science in Semiconductor Processing, 179, 108486. https://doi.org/10.1016/j.mssp.2024.108486

Ramachandran, T., Kalla, R. M. N., Kumar, Y. A., Ghosh, A., Al-Sehemi, A. G., Khan, R., & Lee, J. (2025). Black phosphorus as a multifunctional electrode material for all energy storage devices. Journal of Alloys and Compounds, 182500. https://doi.org/10.1016/j.jallcom.2025.182500

Rastogi, P., Negi, P., Rawat, B. S., Joshi, N. C., Ahmad, W., Kumar, N., & Khati, P. S. (2024). Optical and electrochemical analysis of nitrogen-doped carbon quantum dots from Moosa balbeesiaana peels for advanced supercapacitor applications. Carbon Trends, 16, 100381.

Rajeshwari J., Kishore P.S., Vishwanathan B., Varadarajan T.K. (2009). One-dimensional MoO2 nanorods for supercapacitor applications. Electrochem Commun 11:572–575. https://doi.org/10.1016/j.elecom.2008.12.050

Rajkumar, S., Subha, R., Gowri, S., Bella, A. & Merlin, J. P. (2022). Enhanced electrochemical performance of aminophenol-modified ZnO as electrode material for supercapacitors. *Ionics* https:// doi. org/ 10. 1007/ s11581- 021- 04321-5.

Saraf, M., Rajak, R., & Mobin, S. M. (2016). A fascinating multitasking Cu-MOF/rGO hybrid for high performance supercapacitors and highly sensitive and selective electrochemical nitrite sensors. Journal of Materials Chemistry A, 4(42), 16432-16445. https://doi.org/ 10.1039/C6TA06470A

Sembiring, S., Riyanto, A., Simanjuntak, W., & Situmeang, R., (2017). Effect of MgO-SiO 2 Ratio on the Forsterite (Mg 2 SiO 4) Precursors Characteristics Derived from Amorphous Rice Husk Silica. Oriental Journal of Chemistry. 33. 1828-1836. https://doi.org/10.13005/ojc/330427.

Sharma, S., Devi, M., Kumar, P., Thakur, N., Kumar, K., Jeet, K., Kumar, A., Thakur, N. (2025). Photocatalytic, antibacterial and antioxidant study of Vitex negundo mediated green synthesized nickel and neodymium doped zinc oxide nanoparticles. *Toxicological & Environmental Chemistry*, *107*(1), 178-206.

Shinde, S. K., Dubal, D. P., Ghodake, G. S., Kim, D. Y. & Fulari, V. J. (2016). Morphological tuning of CuO nanostructures by simple preparative parameters in SILAR method and their consequent effect on supercapacitors. Nano-Structures & Nano-Objects, 6, 5-13. https://doi.org/10.1016/j.nanoso.2016.01.004

Shinde, S.K., Ghodake, G.S., Dubal, D.P., Dhaygude, H.D., Kim, D.-Y. & Fulari, V.J. (2017). Enhanced photoelectrochemical properties of nanoflower-like hexagonal CdSe0.6Te0.4: Effect of electron beam irradiation, J. Ind. Eng. Chem. 45 92–98. https://doi.org/10.1016/j.jiec.2016.09.007

Sim, H. T., Gençaslan, M., & Merdan, M. (2024). Synthesis of MgO nanoparticles via the sol-gel method for antibacterial applications, investigation of optical properties and comparison with commercial MgO. Discover Applied Sciences, 6(11). https://doi.org/10.1007/s42452-024-06299-x

Sohouli, E., Teymourinia, H., Ramazani, A., & Adib, K. (2023). Preparation of high-performance supercapacitor electrode with nanocomposite of CuO/NCNO flower-like. Scientific Reports, 13(1), 16221. https://doi.org/10.1038/s41598-023-43430-1

Srimuk, P., Luanwuthi, S., Krittayavathananon, A., & Sawangphruk, M. (2015). Solid-type supercapacitor of reduced graphene oxide-metal organic framework composite coated on carbon fiber paper. Electrochimica Acta, 157, 69-77. https://doi.org/10.1016/j.electacta.2015.01.082

Sundeep, D., Daniel Ephraim, S., Gopala Krishna, A., Ravikumar, R. V. S. S. N., Vijaya Kumar, T., & Pavan, Y. L. (2016). Spectral characterization of mechanically synthesized MoO_3–CuO nanocomposite. International Nano Letters, 6(2), 119–128. https://doi.org/10.1007/s40089-015-0178-z

Taghavi Fardood, S., Ramazani, A., Joo, S. W., & Asiabi, P. A. (2018). A novel green synthesis of copper oxide nanoparticles using a henna extract powder. Journal of Structural Chemistry, 59(7), 1737–1743. https://doi.org/10.1134/s0022476618070302

Thakur, N., & Thakur, N. (2025). Photocatalytic adsorption and scavenging potential of chemical and green encapsulated anatase phase of coupled doped Zn-Co TiO2 nanoparticles. *Journal of Dispersion Science and Technology*, *46*(7), 1071-1086.

Topal Canbaz, G. (2023). Green Synthesis of CuO Nanoparticles Using Tragopogon porrifolius and Their Antioxidant and Photocatalytic Applications. *Cumhuriyet Science Journal*, *44*(4), 671–677. https://doi.org/10.17776/csj.1329389

Verma, N., Pathak, D., & Thakur, N. (2024). Eco-friendly green synthesis of (Cu, Ce) dual-doped ZnO nanoparticles with Colocasia esculenta plant extract using microwave assisted technique for antioxidant and antibacterial activity. *Next Materials*, *5*, 100271.

Verma, N., Pathak, D., Kumar, K., Jeet, K., Nimesh, S., Loveleen, L., Kumar, S., & Thakur, N. (2025). Photocatalytic, antibacterial and antioxidant capabilities of (Fe, Al) double doped ZnO nanoparticles with Murraya Koenigii leaf extract synthesized by using microwave assisted technique. *Materials Chemistry and Physics*, *333*, 130422.

Vinayagar, K., Kandasamy, M., Sivaramasundaram, K., Suresh, S., Almansour, A. I., Pugazhenthiran, N., Kandasamy, M., Kandasamy, M., Karthick Kumar, S., Selvi, J., Muthuchelian, K., & Muthuchelian, K. (2024). Solar to Thermal Energy Conversion Potential of Carbon Nanotubes Modified Copper Oxide Nanocomposite Thin Film Solar Selective Absorbers. *ChemistrySelect*, *9*(27). https://doi.org/10.1002/slct.202401042

Wang Z. L. (2001). Transmission electron microscopy and spectroscopy of nanoparticles, Characterization of Nanophase Materials, Wiley, 37-80. http://dx.doi.org/10.1002/3527600094.ch3

Wang, Y., Lei, Y., Li, J., Gu, L., Yuan, H., & Xiao, D. (2014). Synthesis of 3D-nanonet hollow structured Co3O4 for high capacity supercapacitor. ACS applied materials & interfaces, 6(9), 6739-6747. https://doi.org/10.1021/am500464n

Wei, T., Zhang, Q., Wei, X., Gao, Y. & Li, H., (2016). A facile and low-cost route to heteroatom doped porous carbon derived from Broussonetia papyrifera bark with excellent supercapacitance and CO2 capture performance. Scientific Reports, 6. https://doi.org/10.1038/srep 22646.

Xavier, A. R., Ravichandran, A. T., Vijayakumar, S., Angelin, M. D., Rajkumar, S., & Merlin, J. P. (2022). Synthesis and characterization of Sr-doped CdO nanoplatelets for supercapacitor applications. Journal of Materials Science: Materials in Electronics, 33(11), 8426-8434. https://doi.org/10.1007/s10854-021-06329-z

Yadav, M.S. (2020). Metal oxides nanostructure-based electrode materials for supercapacitor application. *J Nanopart Res* **22**, 367. https://doi.org/10.1007/s11051-020-05103-2

Yoon, Y. S., Cho, W. I., Lim, J. H., & Choi, D. J. (2001). Solid-state thin-film supercapacitor with ruthenium oxide and solid electrolyte thin films. Journal of power sources, 101(1), 126-129. https://doi.org/10.1016/S0378-7753(01)00484-0

Yue, T., Shen, B. & Gao, P. (2022). Carbon material/MnO2 as conductive skeleton for supercapacitor electrode material: A review. *Renew.Sustain. Energy Rev.* 158, 112131. https://doi.org/10.1016/j.rser.2022.112131

Zaidan, B. A. H., Sohouli, E., & Mazaheri, S. (2019). A novel capping agent in preparation and characterization of CuAl2O4/CuO nanocomposite and its application for electrochemical detection of dopamine. Anal. Bioanal. Electrochem, 11(1), 108-122.

Zheng, C., Cao, C., Ali, Z., & Hou, J. (2014). Enhanced electrochemical performance of ball milled CoO for supercapacitor applications. Journal of Materials Chemistry A, 2(39), 16467-16473. https://doi.org/10.1039/C4TA02885F

Zheng, C., Zhou, X., Cao, H., Wang, G. & Liu, Z. (2014). Synthesis of porous graphene/activated carbon composite with high packing density and large specific surface area for supercapacitor electrode material. *J. Power Sour.* 258, 290–296. https://doi.org/10.1016/j.jpowsour.2014.01.056

Publisher's note: Eurasia Academic Publishing Group (EAPG) remains neutral with regard to jurisdictional claims in published maps and institutional affiliations.

Open Access. This article is licensed under a Creative Commons Attribution-NoDerivatives 4.0 International (CC BY-ND 4.0) licence, which permits copy and redistribute the material in any medium or format for any purpose, even commercially. The licensor cannot revoke these freedoms as long as you follow the licence terms. Under the following terms you must give appropriate credit, provide a link to the license, and indicate if changes were made. You may do so in any reasonable manner, but not in any way that suggests the licensor endorsed you or your use. If you remix, transform, or build upon the material, you may not distribute the modified material. To view a copy of this license, visit https://creativecommons.org/licenses/by-nd/4.0/.